



Intercomparison of surface velocimetry techniques for drone-based marine current characterization

Iain Fairley^a, Nicholas King^a, Jason McIlvenny^b, Matthew Lewis^c, Simon Neill^c, Benjamin J. Williamson^{b,*}, Ian Masters^a, Dominic E. Reeve^a

^a Faculty of Science and Engineering, Swansea University Bay Campus, Swansea, SA1 8EN, UK

^b Environmental Research Institute, University of the Highlands and Islands, Thurso, KW14 7EE, UK

^c School of Ocean Sciences, Bangor University, Menai Bridge, Anglesey, LL59 5AB, UK

ARTICLE INFO

Keywords:

Drones
Tidal currents
Surface velocimetry
Particle image velocimetry
Particle tracking velocimetry
Optical flow

ABSTRACT

Mapping tidal currents is important for a variety of coastal and marine applications. Deriving current maps from in-situ measurements is difficult due to spatio-temporal separation of measurement points. Therefore, low-cost remote sensing tools such as drone-based surface velocimetry are attractive. Previous application of particle image velocimetry to tidal current measurements demonstrated that accuracy depends on site and environmental conditions. This study compares surface velocimetry techniques across a range of these conditions. Various open-source tools and image pre-processing methods were applied to six sets of videos and validation data that cover a variety of site and weather conditions. When wind-driven ripples are present in imagery, it was found a short-wave celerity inversion performed best, with mean absolute percentage error (MAPE) of 5–6% compared to surface drifters. During lower wind speeds, current-advected surface features are visible and techniques which track these work best, of which the most appropriate technique depends on specifics of the collected imagery; MAPEs of 9–21% were obtained. This work has quantified accuracy and demonstrated that surface current maps can be obtained from drones under both high and low wind speeds and at a variety of sites. By following these suggested approaches, practitioners can use drones as a current mapping tool at coastal and offshore sites with confidence in the outputs.

1. Introduction

Spatial mapping of tidal currents is important for a range of sectors and research fields. This work focuses on sites related to tidal stream energy extraction (Bahaj, 2011; Khan et al., 2009) where knowledge of currents is vital at all stages of project development, from initial resource assessment (Carpman et al., 2016; Cossu et al., 2021; Murray et al., 2017; Sentchev et al., 2020) to detailed turbine array planning (González-Gorbeña et al., 2018; Frost et al., 2017; Togneri et al., 2016). However, marine surface current information is also important for aquaculture (Brooks et al., 1999; Mente et al., 2006; Sponaugle et al., 2002; Carral et al., 2021), marine pollution assessment (Bellomo et al., 2015; Keramea et al., 2021; Kim et al., 2010), plankton studies (Geyer et al., 2022), sediment transport (Duvall et al., 2019) and other coastal and environmental projects (Rusdiansyah et al., 2018; McIlvenny et al.,

2021; Estournel et al., 2001; Kataoka et al., 2013); the findings presented here are equally applicable to such fields. Traditionally, marine current mapping makes use of vessel mounted transects with in-situ devices, predominantly acoustic Doppler current profilers (ADCPs) (Fairley et al., 2013; Goddijn-Murphy et al., 2013). This approach is reliable and can provide high-quality, accurate data, but comprehensive mapping of an area is inherently difficult since it requires interpolation between transects that are often sparse in both space and time. Moreover, offshore surveys are costly, risky and cannot easily be achieved reactively, such as to rapidly monitor and assess an ongoing pollution incident. More recently, various radar systems have been used to create spatial maps of currents from measurements of wave propagation and principles of wave-current interaction (Bellomo et al., 2015; Bell et al., 2012; Lopez et al., 2020; McCann et al., 2014; Wyatt, 2018; Gacic et al., 2009; Sentchev et al., 2009). This approach is useful in a fixed location,

* Corresponding author.

E-mail addresses: i.a.fairley@swansea.ac.uk (I. Fairley), nicholas.king@swansea.ac.uk (N. King), jason.mcilvenny@uhi.ac.uk (J. McIlvenny), m.j.lewis@bangor.ac.uk (M. Lewis), s.p.neill@bangor.ac.uk (S. Neill), benjamin.williamson@uhi.ac.uk (B.J. Williamson), i.masters@swansea.ac.uk (I. Masters), d.e.reeve@swansea.ac.uk (D.E. Reeve).

<https://doi.org/10.1016/j.ecss.2024.108682>

Received 7 March 2023; Received in revised form 6 February 2024; Accepted 12 February 2024

Available online 13 February 2024

0272-7714/© 2024 The Authors. Published by Elsevier Ltd. This is an open access article under the CC BY license (<http://creativecommons.org/licenses/by/4.0/>).

but the required infrastructure and radar permitting required means mobile instrumentation is less feasible. Satellites have also been used to remotely sense ocean currents (Dohan, 2017; Ubelmann et al., 2021), but with coarse resolution and poor results close to coastlines (Klemas, 2012). Drone based optical surface velocimetry is a complementary technique that can enable very high spatial resolution maps of surface currents to be achieved rapidly and reactively if necessary.

Use of real world optical surface velocimetry has largely focused on the fluvial domain; initially from fixed cameras (Fujita et al., 1998) but more recently from drones (Strelnikova et al., 2020; Streßer et al., 2017; Tauro et al., 2015, 2016) which has enabled reactive measurements and assessment of less accessible sites. Within this sphere, a wide range of open source tools to conduct surface velocimetry have been developed (Pearce et al., 2020). The two most common approaches are large scale particle image velocimetry (Lewis et al., 2015, 2018a, 2018b; Sivas et al., 2015; Sutarto, 2015; Thielicke et al., 2014, 2021; Zhu et al., 2019) (hereafter referred to as PIV), which takes an Eulerian approach, and large scale particle tracking velocimetry (Eltner et al., 2020; Tauro et al., 2019) (hereafter referred to as PTV), which takes a Lagrangian approach. Other methods include variations of PIV optimized for ephemeral features (Leitão et al., 2018), optical flow (Eltner et al., 2020; Tauro et al., 2019), space time image velocimetry (Fujita et al., 2019; Tsubaki et al., 2011) and wave celerity based inversions (Streßer et al., 2017), similar to radar approaches (Bell et al., 2012; McCann et al., 2014; Wyatt, 2018).

Use of optical surface velocimetry at offshore locations has attracted considerably less attention, in part due to the increased complexity of measurements at offshore sites. There are two key differences when comparing offshore sites to fluvial environments: firstly the lack of land in the field of view means georeferencing without ground control is required and secondly there may be fewer and less defined tracers on the water surface to track. The majority of drone-based work in marine environments has been related to surfzone physics (Holman et al., 2017; Wilson et al., 2018; Dérian et al., 2017) or to biophysical interactions further offshore (Lieber et al., 2019, 2021; Waggitt et al., 2016; Slingsby et al., 2022). Rüssmeier et al. (2017) demonstrated that PIV using a fixed camera on a piling could provide reasonable results in a tidal inlet under suitable conditions, which indicated that drone-based approaches further offshore had potential. Until recently, effort had not been applied to testing and validating approaches to allow quantitative studies on tidal currents measured from drones; this validation is required to give practitioners confidence in results. Fairley et al., 2021, 2022, applied LSPIV to three sites and compared results to validation data collected by surface drifters and vessel-mounted ADCP measurements. Land-based georeferencing tests suggested that georeferencing of nadir imagery only using GPS and gimbal information was sufficiently accurate. It was found that when conditions were suitable and turbulent structures were clearly visible on the water surface, velocimetry outputs compared well with measured data. However, when turbulent structures were less obvious, accuracy degraded, and results were poorer for lower velocities. McIlvenny et al. (2022) considered whether an optical flow approach would provide better performance using data from two of the same sites, but had mixed results. Given the range of accuracies obtained, and the strong dependence on site and environmental conditions, it is believed important to test further methods and additional sites compared to these previously reported studies. Space-time image velocimetry is less appropriate for offshore locations as it requires knowledge of the flow direction, which is easy to estimate for a river but less so for the open sea; however, wave celerity based approaches and PTV may perform better than PIV or optical flow under certain conditions and so are worth testing.

The aim of this research is to extend the previous testing of drone-based surface velocimetry for marine surface currents to a greater number of environments, surface velocimetry techniques, and image pre-processing approaches. The open-source approaches tested were PIV (using PIVlab (Thielicke et al., 2021; Thielicke et al., 2014)), PTV (using

TracTrac (Heyman, 2019)), optical flow (using code from McIlvenny et al. (2022)), and a short wave celerity inversion (using CopterCurrents (Streßer et al., 2017)). Two sets of images were tested: a set of contrast stretched greyscale images and the same images that had been binarized. The objective is to provide guidance on the most appropriate open-source approaches for surface current mapping in tidal environments and demonstrate the accuracies that could be expected. This is vital information if drones are to be fully utilised for coastal and offshore research and development.

2. Study sites and experimental conditions

The selected sites are all in the United Kingdom, predominantly around the Welsh coast, with one further site in the Inner Sound of the Pentland Firth, Scotland (Fig. 1). The study sites vary in exposure, and bathymetric complexity which affects the spatial scales of tidal currents and this the required spatial scale of a velocity map (Fig. 2). Variation in site characteristics led to differences in visual characteristics of the collected imagery (Fig. 3). All sites except the Mumbles Head site are at locations that are at or close to areas actively considered for tidal stream energy extraction. Mumbles Head was initially tested as a proof-of-concept site and is a useful inclusion being shallower water than the other sites.

Mumbles Head (Fig. 2D) is a shallow water, intertidal site; on the outgoing tide, water from Swansea Bay is channelled between two islands and fast flowing current jets form. Experiments were conducted from about 1.5 h after high water on March 2, 2021. Minimum water depths in the tested area were 1.5 m, wind speeds were 20 km h⁻¹ (Table 1), with waves of 0.7 m measured at a nearby (6 km) buoy. Signals in the imagery were diverse, with both waves and ripples clearly evident, current-advected foam patches from white capping in the current jet and turbulent structures visible outside of the main current.

Strumble Head is an exposed site on the western end of Cardigan Bay; it can be seen from Fig. 2E that bathymetry drops off rapidly, and there are some large rock outcrops. Similar to Ramsey Sound, it is in a semi-progressive tidal regime with peak currents around 1 h before high and low water and current speeds that exceed 2 m s⁻¹ (Ward, 2018). There has been interest in development of tidal energy at the site by a community group Transition Bro Gwaun (Ward, 2018). Experiments were conducted on November 5, 2021 between 10:00 and 12:30. Low tide was at 13:30 and the tidal range was 4.37 m at Fishguard (6 km to the east), meaning the experiment was conducted towards the time of peak current; however, at peak current the rigid inflatable boat (RIB) used to deploy the drifters could not operate in the region of full flow due to waves from an opposing direction. These waves and white capping against the current were the dominant signals in the imagery, with wind speeds up to 23 km h⁻¹ (Fig. 3b).

Ramsey Sound was the site of the Tidal Energy Ltd Demonstration project in 2015 (OES-Environmental. Ramsey Sound, 2017) and the location is currently being redeveloped by Cambrian Offshore. It is a narrow channel (1–2 km wide) that runs N–S between Ramsey Island and the UK mainland (Figs. 2 and 3) and as such is relatively sheltered from waves and the predominant wind directions. Ramsey Sound is situated in a progressive tidal regime (maximum current synchronous with high and low water), with flood currents to the north and ebb currents to the south. The bathymetry of the Sound is very complex (Fig. 2B) and leads to variation in levels of turbulence between flood and ebb (Togneri et al., 2016). Experiments were conducted on two days (May 12 and 14, 2021) with very similar tides but differing weather conditions: on the 12th, hereafter described as the ‘high wind’ case, it was overcast and wind speeds were at the limits of the drone operation (31 km h⁻¹) whereas on the 14th winds were much lower (10 km h⁻¹) and there was bright sunshine (described as the ‘low wind’ case). This difference in windspeed caused differences in the imagery, with ephemeral surface manifestations of turbulence much clearer in the low wind case (Fig. 3).

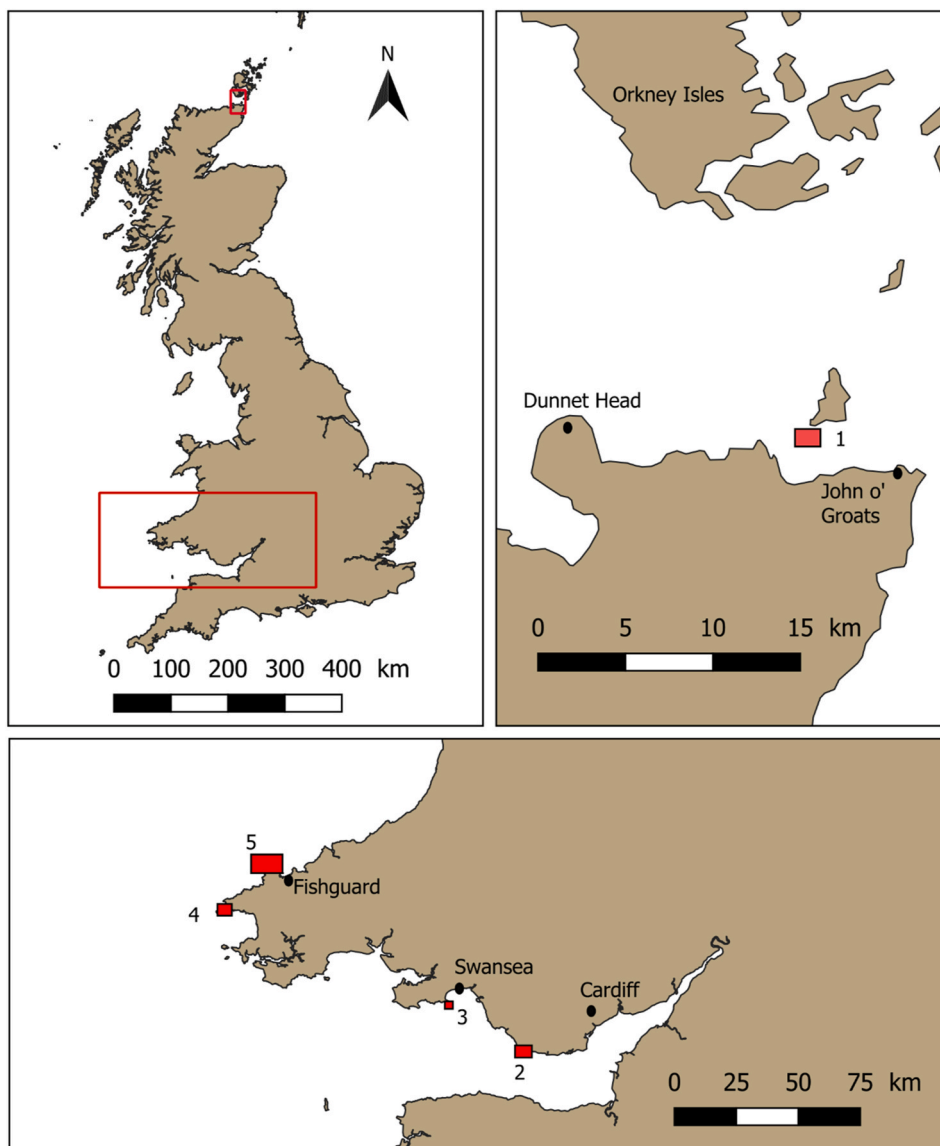


Fig. 1. Location of study sites with the Inner Sound study site marked (1) and sites in South Wales comprising (2) St Donats, (3) Mumbles Head, (4) Ramsey Sound and (5) Strumble Head.

St Donats, on the northern coast of the Bristol Channel is close to the site considered for energy extraction by Willis et al. (2010). At its head, the Bristol Channel has the second highest tidal range in the world and associated strong tidal currents driven by a standing wave regime; at the study site, mean spring ranges are 10 m and mean spring currents exceed 2.5 m s^{-1} (Uncles, 2010). It is exposed to both wind and waves; however, on the test date (August 23, 2021), moderate breezes created ripples but there was minimal wave action. The bathymetry (Fig. 2) is relatively smooth meaning that strong turbulent signals are not generated and instead ripples dominate the imagery (Fig. 3e). The experiment took place on the outgoing tide from 3 h after high water (maximal flow) for 1.5 h; tidal range on the experiment day was 10.64 m at Barry (16 km to east) and 8.35 m at Porthcawl (16 km to west).

The Inner Sound of the Pentland Firth is one of the foremost tidal stream energy extraction sites in the world, being home to the MeyGen Project (Atlantis, 2021) which, with $4 \times 1.5 \text{ MW}$ turbines installed is the largest tidal stream array in the world. Peak currents are in excess of 5 m s^{-1} (Murray et al., 2017) and there are large crevices in the bedrock that generate turbulent features. Previous UAV surveys in the area have mapped substantial kolk boils on the surface (Slingsby et al., 2021), an example of which can be seen in Fig. 3f. Fieldwork was conducted on the

flooding tide on July 2, 2021, wave action was minimal and wind speed was 16 km h^{-1} .

3. Methods

3.1. Flight methodology

Quadcopter drones were used to collect the data, given the requirement for stationary hovering during data collection. A DJI M210v2 RTK drone carrying a Zenmuse X7 camera with a 35 mm lens (image size 2160 x 3824 pixels) was used for all flights at the Welsh sites and a DJI Phantom 4 Pro 2.0 with in-built camera (image size 2160 x 2096 pixels) used at the Inner Sound site in Scotland. Multiple videos covering different current speeds were collected at each site except for the Inner Sound where only one video was recorded.

The flight approach and video recording was as described in Fairley et al. (2022): the drones were hovered at between 100 and 120 m above the sea surface depending on wind conditions, the gimbal directed downwards at -90° (nadir imagery) and the long axis of the image aligned parallel to the main flow direction while 1-min long videos were collected. The maximum permitted flight height for drones is 120 m, and

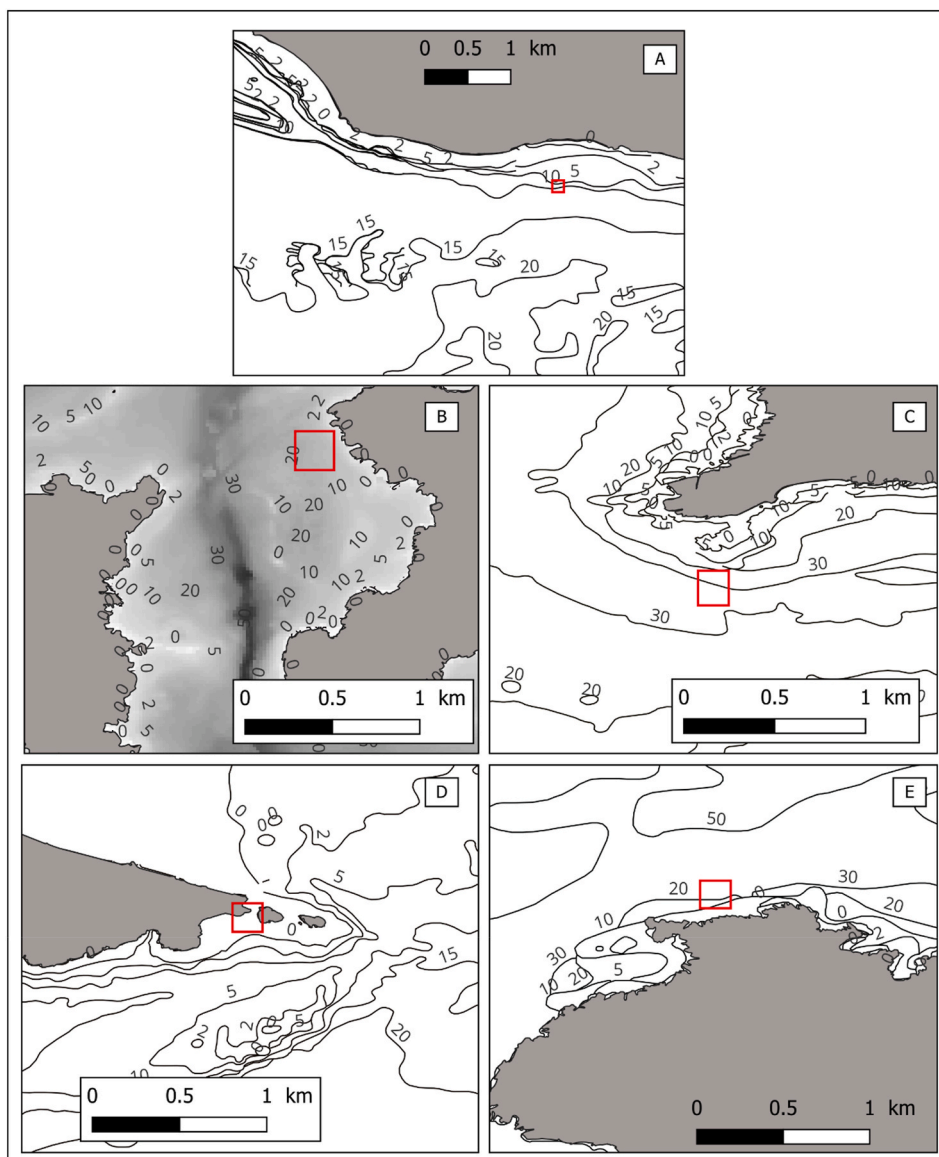


Fig. 2. Bathymetric maps of the 5 study sites: A) St Donats, B) Ramsey Sound, C) Inner Sound, D) Mumbles Head, E) Strumble Head. Depths are shown in metres.

higher flight heights are preferred to give larger image field-of-views; however, maintaining 120 m can be difficult hence the variability in flight heights between recordings. Whilst the vertical hover accuracy of the Phantom Pro 4 is ± 0.5 m with GPS, environmental conditions and GPS signal quality can affect this further. For the Inner Sound site, the Phantom 4 Pro flown at a height of 120 m resulted in 3.29 cm/pixel (image height) and 2.99 cm/pixel (width). For the other sites, the M210 with the Zenmuse X7 camera gave a pixel size of 1.34 cm/pixel at 120 m and 1.12 cm/pixel at 100 m during a windy flight at Ramsey Sound. However, the current extraction techniques account for the height/pixel size changes.

The drones were flown from land close to waterline for the Welsh sites, either from the cliff (Ramsey Sound and Strumble Head) or the beach (St Donats and Mumbles head). At the Inner Sound the drone was flown from a vessel given the distance offshore of the area of interest. It is important to know the drone elevation above the water surface; for the Inner Sound, St Donats and Mumbles, the take-off elevation was taken to be the tidal elevation and hence the elevation above take-off recorded by the drone used. For Ramsey Sound and Strumble head, the elevation of the take-off location was measured and then data from nearby tide gauges used to establish height difference between the water level and

the take off, and then the added to the elevation above take off from the drone to obtain height of drone above the water level. This estimation will introduce error into the velocity estimation since ground pixel size depends on it; however, since the height measurements was measured with RTK GPS and tide gauges are relatively accurate, this error is likely to be substantially less than ± 0.5 m.

3.2. Validation datasets

Validation data were collected using surface drifters for all sites except the Inner Sound where an ADCP transect was used because retrieval of GPS drifters would be problematic in such a large and exposed area of water. The surface drifters were constructed based on a Davis drifter (Davis, 1985) type design with a tarpaulin sail that captured the upper 0.5 m of the water column and had minimal windage (Fairley et al., 2022). Low cost Garmin Etrex 10 GPS units were attached to the drifters in a dry bag and used to record position at a regular interval (1 s for Mumbles Head, 2 s for all other sites) and change in position then converted to velocity. While absolute accuracy of these devices is relatively low (~ 5 m), previous studies have shown that short-term relative accuracy is much higher, and velocities can be

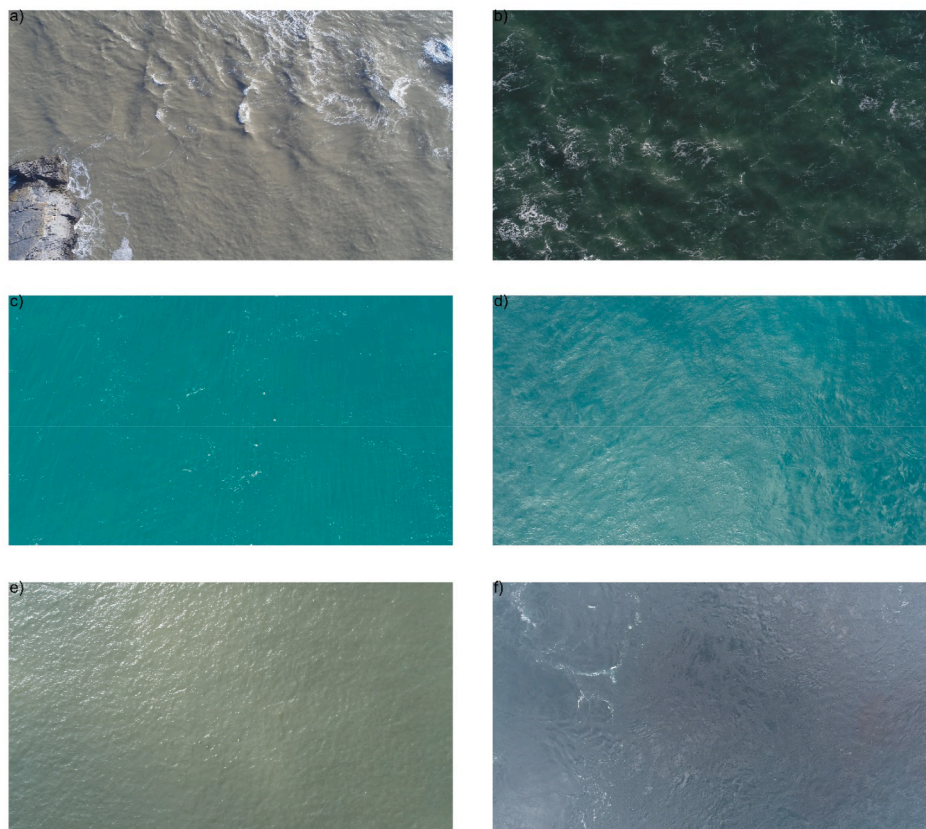


Fig. 3. Example raw images from the different sites and conditions: a) Mumbles Head; b) Strumble Head; c) Ramsey Sound, low wind; d) Ramsey Sound, high wind; e) St. Donats; f) Inner Sound. Image dimensions are approximately 120 m by 60 m (exact dimensions depending on flight height).

Table 1
Dates and wind conditions at each location.

Site	Date	Drone	Wind speed (km h ⁻¹)	Wave height (m)
Mumbles Head	02/03/21	M210 RTK	20	0.7
Strumble Head	05/11/21	M210 RTK	23/gust 40	0.9
Ramsey Sound	12/05/21	M210 RTK	31	1.3
	14/05/21	M210 RTK	10	0.2
St Donats	23/08/21	M210 RTK	13	0.2
Inner Sound	02/07/21	P4 Pro 2.0	16	0.3

obtained with good accuracy using change of position (Schaefer et al., 2015; Townshend et al., 2008; Witte et al., 2004, 2005). Previous studies using similar units have suggested that the majority of speed errors are within $\pm 0.2 \text{ m s}^{-1}$, and a mean error of 0.01 m s^{-1} has been reported (Fairley et al., 2022). Drifters were deployed using a RIB upstream of the area of interest and then collected by the same RIB and taken upstream before being re-deployed. 15 drifter tracks were used at the sites where drifters were deployed.

At the Inner Sound, a 7 m catamaran was used to conduct an ADCP transect after the drone flight (which was conducted from the same vessel). A Teledyne Workhorse Sentinel 600 kHz, configured to alternate between current measurement and bottom track pings at 2 Hz, was used and differential GPS positioning used from the vessel positioning system. Only the top bin of the ADCP profile was considered; based on instrument depth and bin size this meant the velocity between 2.66 and 4.66

m below the surface was used as validation.

3.3. Image pre-processing

The ripple inversion approach made use of raw video imagery. For all other approaches, two different sets of images using frames extracted from the video were tested. Firstly, while the video captured frames at 30 fps, every other frame was extracted so the frame rate was 15 fps (66.67 ms temporal separation of images). The motivation for this was to reduce the current speed associated with a feature movement of 1 pixel between frames (from 0.9 m s^{-1} to 0.45 m s^{-1} for the DJI M210v2 RTK). It also sped up processing time due to fewer images being used. The first set of images, described as 'normal' going forward, were transformed to greyscale, contrast stretched with a saturation of 2% and then contrast limited adaptive histogram equalization, or CLAHE, (Zuiderverld and Heckbert, 1994) applied with a square window of 40×40 pixels. This window size was based on sensitivity testing (Fairley et al., 2021). CLAHE is used to increase the contrast of the image; by computing histograms for each window, it allows for good performance even in images with spatially variable properties. The second set of images, described as 'binarized' were the normal set of images that were subsequently binarized using the MATLAB *imbinarize* command with default settings. The original motivation for testing this was the desire to minimise the influence of background signals which were typically more subdued than turbulent features but were at times the dominant feature. An example of this difference from Strumble Head is given in Fig. 4, where wave motion induced signatures are removed by binarization.

3.4. Current extraction approaches

For all current extraction methods, 1-min average velocities were calculated for the average of all-inter frame velocities, whereby a

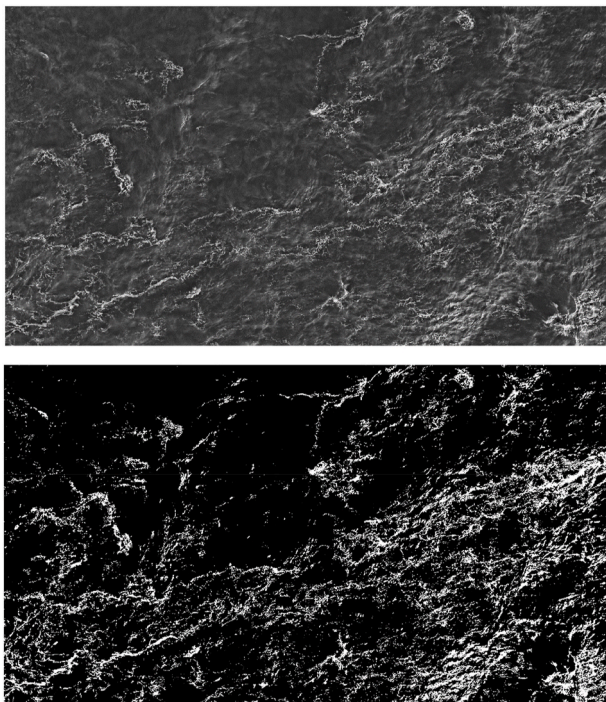


Fig. 4. An example from Strumble head showing the difference between the 'normal' (top) and 'binarized' (bottom) image sets. Image dimensions are approximately 120 m by 60 m.

velocity vector set is generated for between each video frame (15 frames per second) then all the vectors averaged to generate the 1-min average vector.

3.4.1. Large scale particle image velocimetry

Large scale particle image velocimetry was conducted using the open source PIVlab toolbox (Thielicke et al., 2014, 2021). The approach used has been described in detail in Fairley et al. (2022): default settings (correlation robustness and sub pixel estimator) were used except for interrogation area sizes which were set as a three pass analysis using windows of 128, 64, 32 pixels based on sensitivity testing, with velocity vectors being generated for each 32*32 pixel box (Fairley et al., 2021). Differing-size windows are used to capture faster-moving particles (large window) and slower moving particles in each window frame. While PIVlab does allow for image pre-processing, this was not used as pre-processing had been done prior to the analysis (section 3.3). Post-analysis, temporal averages of the frame-on-frame results were taken to provide a 1-min mean current.

3.4.2. Particle tracking velocimetry

The open-source TracTrac PTV software (Heyman, 2019) was used in this study; the primary motivation for using this software was that, unlike some other PTV codes, image binarization was not a requirement. Equally, good performance of the software has been shown for a range of fluvial applications (Duguay et al., 2022; Omoniyi et al., 2021; Schnauder et al., 2022). TracTrac was run with default parameters, except for the 'blob scale', which defines the expected size of particles and was increased from the default 1.2 pixels to 3 pixels based on testing with a subset of the data, with velocity vectors generated for each 3*3-pixel box.

3.4.3. Optical flow

A short script was written in MATLAB using the Farneback optical flow algorithm (Farneback, 2003). The Farneback method is a two-frame dense optical flow method using quadratic polynomials to

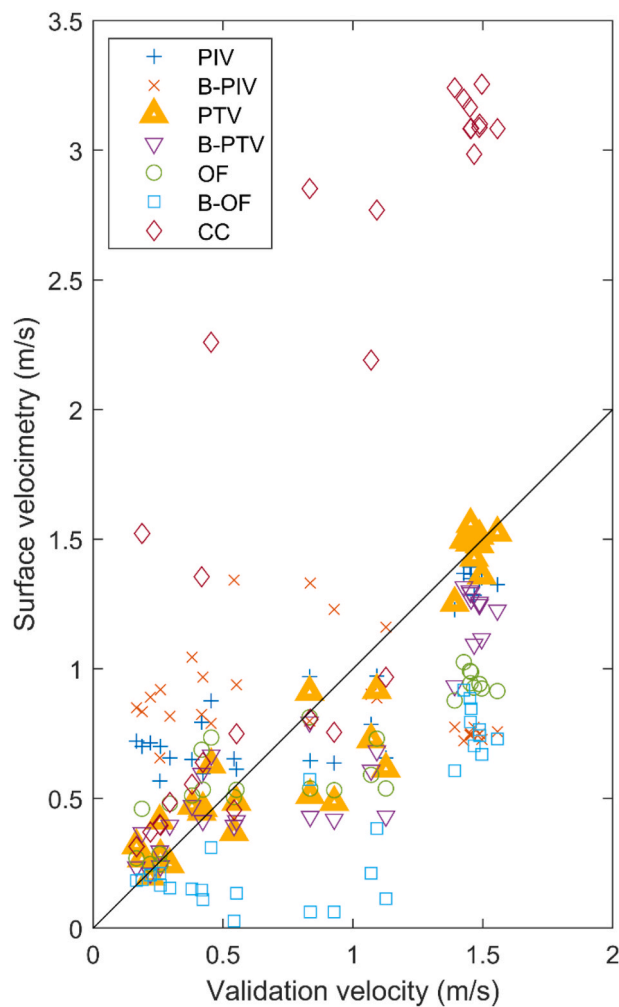


Fig. 5. Scatter plots of surface velocimetry estimate against validation velocity for Mumbles Head. In the legend, the 'B-' prefix refers to results using the binarized images, 'CC' refers to CopterCurrents and 'OF' to optical flow, PIV and PTV are the standard acronyms. The approach that performed best (lowest MAPE) is marked in bold (PTV, yellow triangle). The black solid line is the 1:1 line.

derive the motion between the frames. The following settings were used: number of pyramid levels: 3, neighbourhood size: 3, filter size: 15 and iterations: 3. The Farneback method employs a pyramid-based scheme detecting changes in pixel position at a number of resolutions. This has the advantage of being able to measure large velocity changes. Results of individual two frame comparisons were stored in a matrix and then results averaged for the whole video sequence to estimate average flow speeds over a 1-min video sequence. Vectors were generated for each 15*15-pixel square.

3.4.4. Ripple inversion approach

CopterCurrents (Streßer et al., 2017) is a software package that uses video footage from aerial drones of a body of water to estimate the surface currents. This is achieved using linear wave theory to calculate the theoretical velocity of a surface wave, assuming it is unaffected by currents, this is then subtracted from the actual measured velocity of the wave to determine the underlying currents.

The first stage of this method is to assign pixel coordinates from the video to a rectilinear grid on the surface of the water. Image area is calculated using the effective field of view of the camera and georectified using EXIF data. The image is divided into cells with a given length and width. These cells are extracted and converted to the spectral

Table 2

Root mean square errors, in m s^{-1} , and mean absolute percentage error (%), given in brackets, for the various sites and approaches for current speed. The best performance for each site/condition is highlighted in green.

Site	Velocimetry approach						
	PIV	PIV B	PTV	PTV B	Optical Flow	Optical Flow binarized	Ripple inversion
Mumbles Head	0.29 (65)	0.59 (106)	0.18 (21)	0.28 (28)	0.38 (38)	0.58 (52)	1.22 (123)
Strumble Head	0.52 (25)	0.28 (11)	0.59 (25)	0.32 (14)	0.95 (47)	1.51 (74)	1.06 (54)
Ramsey Low wind	0.14 (12)	0.15 (14)	0.23 (17)	0.21 (18)	0.42 (28)	0.91 (73)	1.26 (116)
Ramsey High wind	0.40 (41)	0.38 (37)	0.47 (50)	0.46 (48)	0.77 (83)	0.81 (87)	0.10 (6)
St Donats	0.52 (33)	0.53 (37)	0.39 (27)	0.41 (29)	0.64 (40)	0.79 (55)	0.07 (5)
Inner Sound	0.52 (24)	0.51 (19)	n/a	n/a	0.35 (14)	0.31 (9)	1.03 (52)

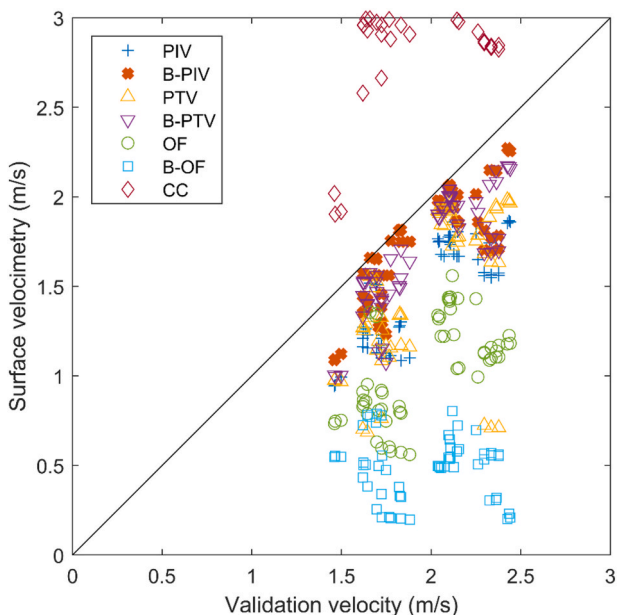


Fig. 6. Scatter plots of surface velocimetry estimates (from drone) against validation velocity (from surface drifters) for Strumble Head. In the legend, the ‘B-’ prefix refers to results using the binarized images, ‘CC’ refers to Copter-Currents and ‘OF’ to optical flow, PIV and PTV are the standard acronyms. The approach that performed best is marked in bold (B-PIV), based on lowest MAPE. The black solid line is the 1:1 line.

domain using 3D Fast-Fourier-Transformation. Using the linear dispersion relation for surface gravity waves in ambient currents:

$$\omega = \sqrt{g|k|\tanh(|k|d)} + k \bullet U$$

Where ω is radial frequency, k is the wave number, d is water depth and U is the current vector. The signal to noise ratio is then calculated for the spectral bins for energy belonging to waves and noise. Maximising this within a given range produces the most likely current speed (Streßer et al., 2017). This toolbox was used with default settings except for the window size was set to 10 m and the signal to noise thresholds removed. Velocity vectors were generated for each 10 m * 10 m-pixel box.

4. Results

In this section, accuracy results are described on a site-by-site basis, contrasting the different velocimetry techniques. For some videos, a certain approach failed to produce results and so these videos were excluded from all the techniques to ensure like-with-like statistics. The exception to this was the Inner Sound, where only one video was available and so the particle tracking method, which failed to track any particles (due to the size of turbulent features), was excluded. For all surface drifter results, average values over drifter tracks in the video field of view were used rather than individual instantaneous velocity data points, this provides some spatio-temporal averaging and so better fits with the 1-min average surface velocimetry results.

Fig. 5 shows scatter plots of the different surface velocimetry techniques against the validation drifter speeds for Mumbles Head. Binarized PIV, optical flow and binarized optical flow showed largely horizontal trends, which indicated poor performance. The CopterCurrents results were very poor, with a significant number of large overpredictions. The PIV results showed good agreement at higher velocities but

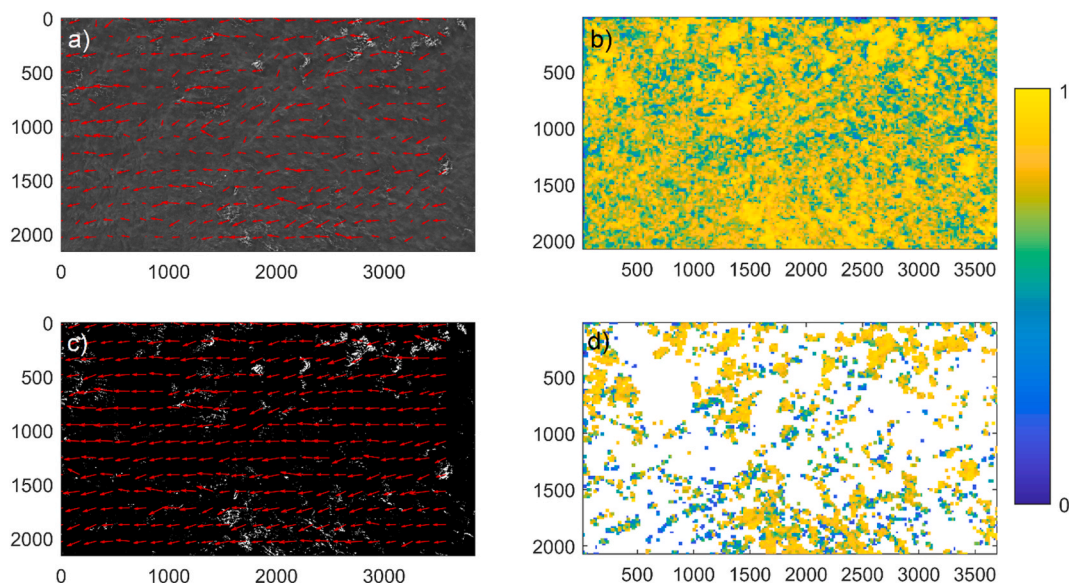


Fig. 7. Example estimated current vectors overlaid on the corresponding images and maps of correlation co-efficient from Strumble Head: a) current vectors from PIV with the normal images; b) correlation coefficients for the normal image; c) current vectors for the binarized images; d) correlation coefficients for the binarized images. The correlation coefficient is shown according to the colour bar. White space in the correlation map indicates no correlation at that point. All results displayed in pixel coordinates (2160*3824; 2.49 cm/pixel).

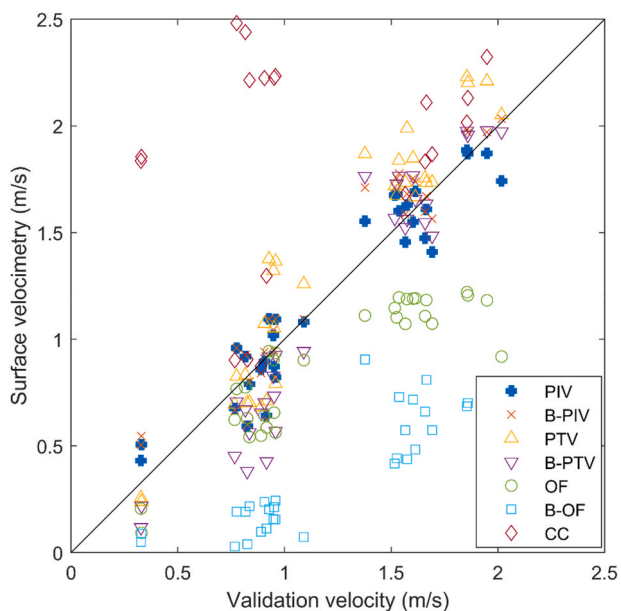


Fig. 8. Scatter plots of surface velocimetry estimate against validation velocity for Ramsey Sound under low wind conditions. In the legend, the ‘B-’ prefix refers to results using the binarized images, ‘CC’ refers to CopterCurrents and ‘OF’ to optical flow, PIV and PTV are the standard acronyms. The approach with lowest MAPE is marked in bold (PIV). The black solid line is the 1:1 line.

overpredicted at lower velocities. By contrast, both the PTV and Binarized PTV results performed well at both high and low velocities, the PTV results using the normal images gave the best statistics (RMSE = 0.18 m s⁻¹ and MAPE of 20%, see Table 2).

At Strumble Head (Fig. 6), all surface velocimetry techniques underestimated the measured surface velocities, with the exception of CopterCurrents which, similar to at Mumbles Head, greatly overestimated flow speeds. The worst performing was optical flow with binarized images, which did not correlate with measured velocities. The other approaches all correlated with measured velocities but at various

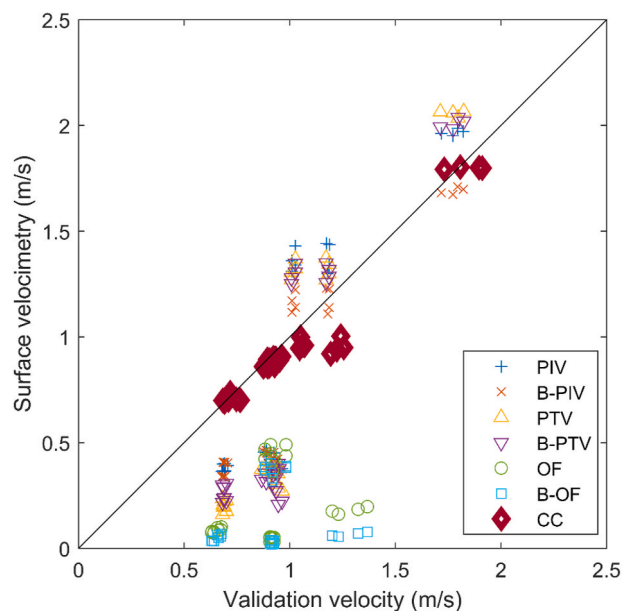


Fig. 9. Scatter plots of surface velocimetry estimate against validation velocity for Ramsey Sound under high wind conditions. In the legend, the ‘B-’ prefix refers to results using the binarized images, ‘CC’ refers to CopterCurrents and ‘OF’ to optical flow, PIV and PTV are the standard acronyms. The approach that performed best with lowest MAPE is marked in bold (CC). The black solid line is the 1:1 line.

levels of under estimation. Both PIV and PTV approaches performed similarly, analysis using the normal set of images gave RMSEs of 0.52 m s⁻¹ and 0.59 m s⁻¹ respectively, and the binarized images improved results to RMSEs of 0.28 m s⁻¹ and 0.32 m s⁻¹ respectively. The underestimation of current speeds is attributed to the presence of other signals such as waves leading to correlations not associated with current signals. While the other optical signals are less intense than turbulent signals or foam traces, in the absence of either of these, the algorithms will track other features which reduced the mean velocity when the

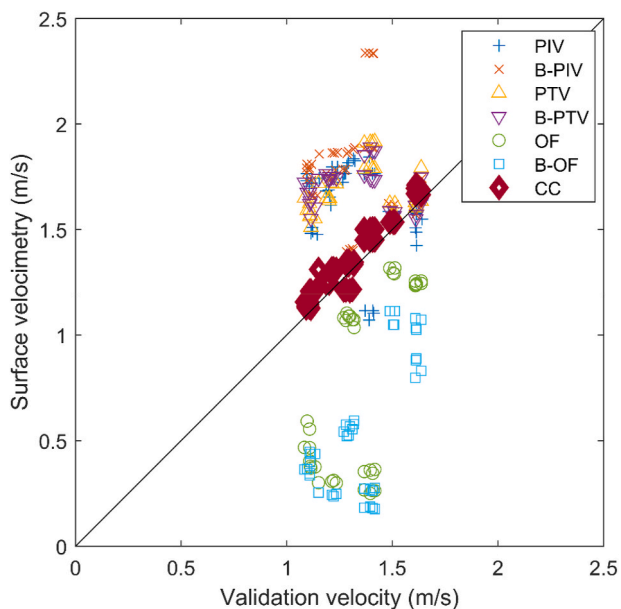


Fig. 10. Scatter plots of surface velocimetry estimate against validation velocity for St Donats. In the legend, the ‘B-’ prefix refers to results using the binarized images, ‘CC’ refers to CopterCurrents and ‘OF’ to optical flow, PIV and PTV are the standard acronyms. The approach with lowest MAPE is marked in bold (CC). The black solid line is the 1:1 line.

average over 1 min is taken. Binarization removes background signals, preventing spurious correlation. An example of this is shown in Fig. 7, which shows the same set of two frame results for both the normal and binarized images. When the binarized set is used, unless there is a clear signal, no correlation can be obtained and no velocity returned, therefore vectors at points without clear signatures were based on interpolation between strong signals. This improves results when averaged over the 1 min.

At Ramsey Sound, under low winds (Fig. 8), PIV and PTV both gave good results, accurately estimating across the measured velocity range. PIV performs better (RMSEs of 0.14/0.15 m s⁻¹ for PIV compared to 0.23/0.21 m s⁻¹ for PTV). In both cases, there is little difference between the normal and binarized image sets due to the lack of other signals in the imagery beyond the turbulent structures. Optical flow results using

the normal images fit well with the 1:1 line for lower velocities but underestimated as measured velocities increase over 1 m s⁻¹. Using binarized images, optical flow always underestimated. CopterCurrents produces good current estimates for some videos but equally there are many cases where currents were overestimated.

Under higher wind conditions at Ramsey Sound (Fig. 9), there were much larger errors for the PIV and PTV approaches due to the turbulent structures being obscured by wind-driven ripples, however the clear presence of these ripples allowed CopterCurrents to provide very good surface current estimates (RMSE = 0.10 m s⁻¹). Errors in PIV/PTV were primarily at lower velocities, for validation velocities between 1 and 1.5 m s⁻¹, there is a split between slight overestimation, which occurred on the flood tide, and underestimation which occurred on the ebb. Fairley et al. attributed this to differences in antecedent bathymetry affecting number of turbulent structures (Fairley et al., 2022). Analysis using binarized images was similar (2–4% difference in percentage error) to analysis with the normal image set (better for PIV and PTV, worse for optical flow).

The test at St Donats also produced best results with CopterCurrents (MAPE = 5%). No other method performed as well; with MAPEs between 27 and 55% (see Fig. 10). This is unsurprising given the dominance of ripples in the collected imagery and minimal other signals.

The final dataset is for the Inner Sound of the Pentland Firth. It is important to recall that for this site, an ADCP transect rather than surface drifters were used for the validation data. Since only one video was available and only one ADCP transect, the top bin of individual ADCP transect measurements were used for validation rather than any averaged value. This affects the results in several ways: firstly, the top bin spanned 2.66–4.66 m below the water surface and so did not measure the true surface velocity; secondly the ADCP transect was collected 20 min after the drone flight and so drone and validation data were not synchronous. Where surface drifter and ADCP data were both available for the same video, Fairley et al. (2022) have shown that surface drifter data provides a better comparison. The temporal separation meant that the presence of a transient jet affected results (Fig. 11). This transient jet of faster flow was identified during video capture in the experiment region with generally lower validation velocities, but was not observed during the ADCP transect: the location of this jet matched datapoints with large overpredictions and hence errors (east of 491850 m in Fig. 11). Therefore, this section of results was removed from the scatter plots and calculations of error statistics.

Nonetheless, good results were still obtained at the Inner Sound for some surface velocimetry techniques (Fig. 12). PIV and optical flow

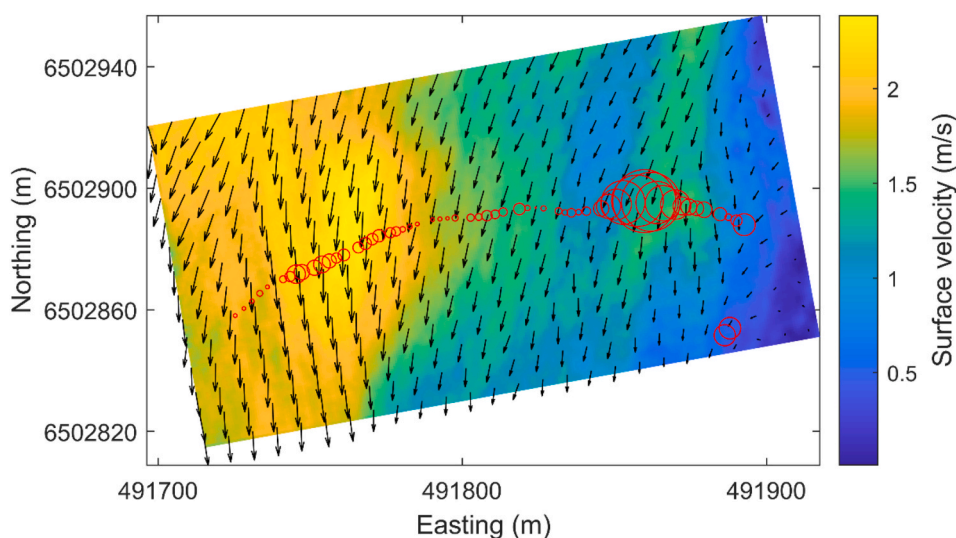


Fig. 11. A map of 1 min mean surface current speeds from the Inner Sound with the transient jet noted during the experiment evident at 491880 m E. The validation points are overlaid as red circles, with larger circles indicating larger percentage errors. Vectors calculated with PIVlab.

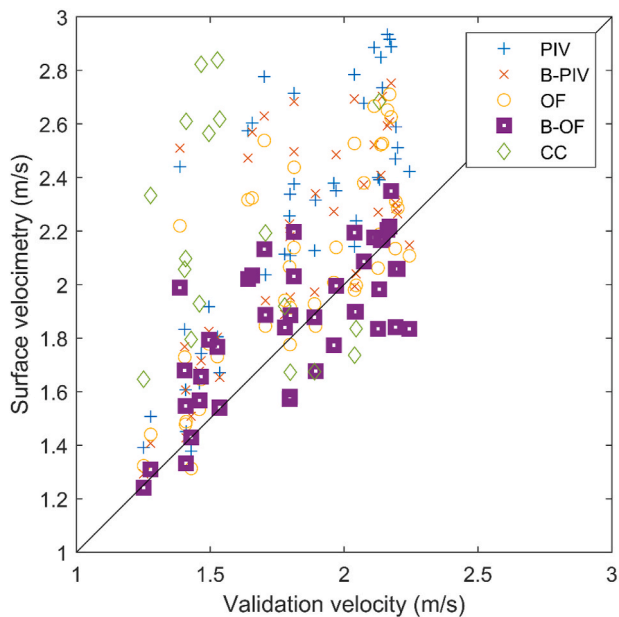


Fig. 12. Scatter plots of surface velocimetry estimate against validation velocity for the Inner Sound. In the legend, the ‘B-’ prefix refers to results using the binarized images, ‘CC’ refers to CopterCurrents and ‘OF’ to optical flow, PIV and PTV are the standard acronyms. The approach with lowest MAPE is marked in bold (B-OF). The black solid line is the 1:1 line.

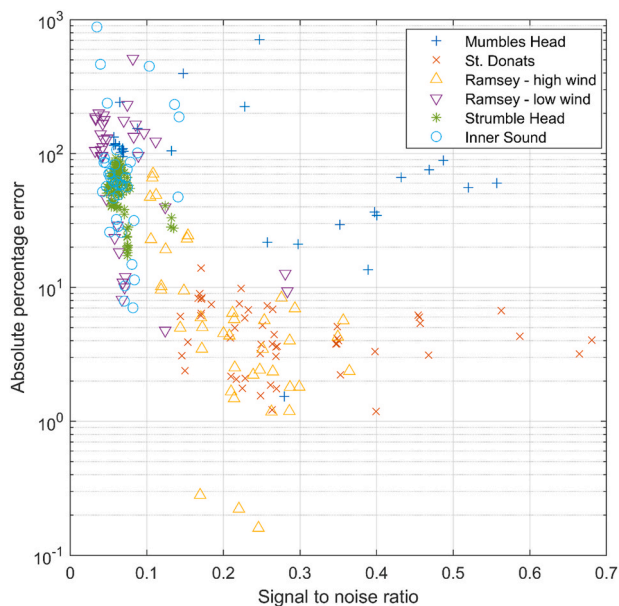


Fig. 13. A plot of absolute percentage error, on a log scale, against signal to noise ratio for the CopterCurrents results at all sites.

performed reasonably well with both sets of images, although there was a positive bias, between 0.045 and 0.44 m s^{-1} , to the results in all cases. There was a reduction in bias and hence an improvement in error statistics for both binarized sets of images. The best performing was the binarized optical flow results with a mean absolute percentage error of 9%. The CopterCurrents results were poor (mean absolute percentage error of 52%) with no obvious trend to the scatter distribution. Interestingly, neither sets of images applied to the PTV approach was able to identify distinct particles and hence produce results, despite testing with a range of analysis parameters (particularly expected size of particle). It is believed this is due to the size of the kolk boils that are the key feature

in these images (e.g., top left of Fig. 3f). It is the size and coherence of these structures between frames that means for the Inner Sound, optical flow outperforms PIV, as described by McIlvenny et al. (2022).

Better error statistics were obtained for the two cases where CopterCurrents performs best, compared to the best case estimates when other methods perform better for a site. This suggests that when ripples are present, a wave celerity type approach is most appropriate for offshore environments. It is believed this is because the presence of ripples can be assumed to be consistent in time and space, compared to the spatio-temporal sparseness of ephemeral surface textures generated by turbulence. In this study, signal to noise ratio (SNR) thresholds, the default setting in CopterCurrents, were removed to generate results for as many videos as possible; however, Fig. 13 shows that use of a SNR threshold would screen out poorly performing results and allow for confidence in estimated velocities in the absence of validation data. For the results here, setting the SNR threshold to 0.15 would remove most results with errors over 10% and keep most results with errors less than this. The exception is the Mumbles Head results where greater errors were evident even for higher SNRs; this may be related to the fact at this site there were larger waves present and shallow water.

5. Discussion

This research has shown that drone-measured tidal currents can be accurate over a broader range of conditions than previously reported. This facilitates greater use of drones for a variety of research and development activities as performance has been quantified over this extended range of conditions. Wide area mapping is feasible in one flight due to the short (1 min) video segments required; mapping can be automated through provision of a set of waypoints. This enables future quantitative work such as tidal energy resource mapping, investigation into the physics of fine scale hydrodynamics of high energy flows and wake mapping at real tidal turbine deployments. Fairley et al. (2022) also demonstrated that, if bathymetric data are available, currents at depth can be estimated with good accuracy using a $1/7$ th power law, which widens the applicability of drone-measured current maps.

It was shown that when ripples dominate, very good ($\text{MAPE} = 5\text{--}6\%$) accuracies can be obtained using CopterCurrents. However, when ripples do not dominate there is not an alternative technique that clearly dominates. McIlvenny et al. (2022) postulated that optical flow techniques only work well when there are not signals moving in differing directions, since that violates one of the assumptions of optical flow. This study corroborates that over a wider range of sites and conditions; the technique only performed best at the Inner Sound where large turbulent structures were advected by the current over an otherwise featureless sea surface. For this site optical flow performed much better than other approaches and so the method should not be dismissed as being limited in application to only this sort of image set. At Ramsey Sound for the low wind case, where smaller scale turbulent features dominate, PIV performed slightly better than PTV. It is postulated that the transient nature of these small-scale features mean identification of tracers through multiple frames, as required for PTV, is not always achievable.

Binarization improves results at Strumble Head and at the Inner Sound, while making minimal difference for the low wind case at Ramsey Sound. As described, this is because when clear signals are visible, binarization can reduce spurious correlations/tracks caused by secondary features, while preserving the dominant signal. It is only for Mumbles Head where binarization worsens results (by 7% for PTV and by 41% for PIV). For the low wind case at Ramsey Sound, the main contaminating signal is sun glint and this is bright enough not to be removed by binarization and is in some frames enhanced. Likewise at Mumbles Head, sun glint is evident and binarization emphasizes the wave signature to increase sun glint on the slope of waves angled towards the sun. Moreover, variable lighting levels caused oversaturation in some frames leading to large white areas when binarized. Thus, basic

binarization is best applied to videos with consistent and diffuse lighting (i.e. uniform cloud). Further development could potentially improve accuracy or confidence in accuracies by utilizing more sophisticated image pre-processing. Removing gradients in lighting intensity over an image, or through time may improve binarization. Empirical mode decomposition was tested as a means of subduing background signals, particularly waves (Fairley, 2021), but was found to be very computationally intensive and so was not pursued; other similar methods might be more fruitful.

While CopterCurrents provides the signal-to-noise ratio as an indication of the quality of the velocities, future research could consider a quality or uncertainty/confidence metric for the other techniques – for example, previous studies have quantified the number of edge pixels when evaluating the relative performance of optical flow and PIV techniques (McIlvenny et al., 2022).

Given the initial similarity between Mumbles Head and Strumble Head in terms of image characteristics, but the differences in appropriate technique, it is worth paying further attention to the two cases. At Strumble Head image characteristics are fairly uniform throughout the image whereas at Mumbles Head there is a clear distinction between regions of white capping induced foam patches and regions where more ephemeral signals are advected by the current, but which are somewhat obscured by features associated with waves. As described in the previous paragraph, the poor results for Mumbles Head with binarized images are probably related to crude binarization rather than the non-binarized image set providing better targets. At Strumble Head, the difference between PIV and PTV is small (0.04 m s⁻¹ difference in RMSE/3% difference in MAPE for the binarized case) whereas at Mumbles Head, the difference is slightly larger (0.11 m s⁻¹ difference in RMSE/44% difference in MAPE). The large difference in MAPE in this case is due to MAPE being affected by large errors for measurements that approach zero, something that was noted at Mumbles Head for the PIV runs. It is suspected that the difference between PIV and PTV at Mumbles is caused by spurious correlations for PIV in the low signal region and were a more sophisticated binarization might generate results more similar to Strumble Head. However, from a practical perspective, given the similarity between PTV and PIV for Strumble Head, PTV is suggested as most appropriate for this type of imagery.

6. Conclusion

This research shows that drone-based surface velocimetry is a useful tool for marine and coastal studies and can provide suitably accurate results over a wider range of conditions than previously reported when providing rapid spatial characterisation of a site. However, the most appropriate technique depends on site characteristics and environmental conditions. A range of surface velocimetry with normal and binarized images were tested and results compared to measured validation data.

The most accurate results were found when short waves dominate (St Donats and the high wind case at Ramsey Sound in this study) and a wave celerity based technique can be used: in these cases RMSEs are less than 0.1 m s⁻¹ which equates to mean absolute percentage error of less than 6%. While this approach does not work well at all sites, a signal to noise threshold can be set to ensure poor results are screened out; a threshold of 0.15 is suggested for offshore locations based on the results in this study.

For the cases where a ripple-based approach was not appropriate, there was no single best alternative, although for each site, accurate velocimetry results could be obtained with the correct method. At sites such as the Inner Sound, with very large turbulent structures (e.g., kolk boils) and where all signals are moving with the current, an optical flow approach using binarized images is suggested (mean absolute error at the Inner Sound of 9%). For cases with smaller turbulent features and limited other signals, such as the low wind Ramsey Sound case, use of particle image velocimetry (PIV) and un-binarized images is most

accurate (mean absolute error of 12%), although PIV and particle tracking velocimetry (PTV) accuracies with both sets of images were similar. For environments with mixed signals including waves and current signals (Mumbles Head and Strumble Head in this study), expert judgement is required based on visual assessment of frame-on-frame images; one site showed best performance with PIV using binarized images (mean absolute percentage error of 11%) whereas the other showed best performance using non binarized PTV (mean absolute percentage error of 21%). It is postulated that a more sophisticated approach to image binarization might reduce this discrepancy.

CRediT authorship contribution statement

Iain Fairley: Writing – original draft, Visualization, Methodology, Investigation, Funding acquisition, Formal analysis, Data curation, Conceptualization, Software. **Nicholas King:** Investigation, Data curation, Methodology. **Jason McIlvenny:** Writing – review & editing, Writing – original draft, Visualization, Software, Methodology, Investigation, Formal analysis, Data curation. **Matthew Lewis:** Writing – review & editing, Formal analysis, Funding acquisition, Resources. **Simon Neill:** Writing – review & editing, Funding acquisition, Resources, Supervision. **Benjamin J. Williamson:** Writing – review & editing, Project administration, Funding acquisition, Conceptualization, Investigation, Methodology, Resources, Supervision. **Ian Masters:** Writing – review & editing, Supervision, Project administration, Funding acquisition, Conceptualization. **Dominic E. Reeve:** Writing – review & editing, Supervision, Project administration, Funding acquisition, Conceptualization, Methodology.

Declaration of competing interest

The authors declare that they have no known competing financial interests or personal relationships that could have appeared to influence the work reported in this paper.

Data availability

Data will be made available on request.

Acknowledgements

The financial support of the Selkie Project is acknowledged. The Selkie Project is funded by the European Regional Development Fund through the Ireland Wales Cooperation programme. The authors would also like to acknowledge the financial support of the EPSRC Supergen ORE Hub (EP/S000747/1) funded V-SCORES project and the support of SEEC (Smart Efficient Energy Centre) at Bangor University, part-funded by the European Regional Development Fund (ERDF), administered by the Welsh Government. M Lewis also wishes to acknowledge the EPSRC fellowship METRIC: EP/R034664/1. We gratefully acknowledge the constructive comments from reviewers.

References

- Atlantis, S., 2021. Meygen tidal energy project, 29/11/2021. <https://simecatlantis.com/projects/meygen/>.
- Bahaj, A.S., 2011. Generating electricity from the oceans. *Renew. Sustain. Energy Rev.* 15 (7), 3399–3416.
- Bell, P.S., Lawrence, J., Norris, J.V., 2012. Determining currents from marine radar data in an extreme current environment at a tidal energy test site. In: 2012 IEEE International Geoscience and Remote Sensing Symposium. IEEE, pp. 7647–7650.
- Bellomo, L., et al., 2015. Toward an integrated HF radar network in the Mediterranean Sea to improve search and rescue and oil spill response: the TOSCA project experience. *Journal of Operational Oceanography* 8 (2), 95–107.
- Brooks, D.A., Baca, M.W., Lo, Y.T., 1999. Tidal circulation and residence time in a macrotidal estuary: cobscook Bay, Maine. *Estuar. Coast Shelf Sci.* 49 (5), 647–665.
- Carpman, N., Thomas, K., 2016. Tidal resource characterization in the folda fjord, Norway. *International Journal of Marine Energy* 13, 27–44.

- Carral, L., et al., 2021. Configuration methodology for a green variety reef system (AR group) based on hydrodynamic criteria - Application to the Ria de Ares-Betanzos. *Estuarine Coastal and Shelf Science*, p. 252.
- Cossu, R., et al., 2021. Tidal energy site characterisation in a large tidal channel in Banks Strait, Tasmania, Australia. *Renew. Energy* 177, 859–870.
- Davis, R.E., 1985. Drifter observations of coastal surface currents during CODE: the method and descriptive view. *J. Geophys. Res.: Oceans* 90 (C3), 4741–4755.
- Dérian, P., Almar, R., 2017. Wavelet-based optical flow estimation of instant surface currents from shore-based and UAV videos. *IEEE Trans. Geosci. Rem. Sens.* 55 (10), 5790–5797.
- Dohan, K., 2017. Ocean surface currents from satellite data. *Journal of Geophysical Research-Oceans* 122 (4), 2647–2651.
- Duguay, J., Biron, P., Buffin-Bélanger, T., 2022. Large-scale turbulent mixing at a mesoscale confluence assessed through drone imagery and eddy-resolved modelling. *Earth Surf. Process. Landforms* 47 (1), 345–363.
- Duvall, M.S., Wiberg, P.L., Kirwan, M.L., 2019. Controls on sediment suspension, flux, and marsh deposition near a bay-marsh boundary. *Estuar. Coast* 42 (2), 403–424.
- Eltner, A., Sardemann, H., Grundmann, J., 2020. Technical Note: flow velocity and discharge measurement in rivers using terrestrial and unmanned-aerial-vehicle imagery. *Hydrol. Earth Syst. Sci.* 24 (3), 1429–1445.
- Estournel, C., et al., 2001. The Rhone river plume in unsteady conditions: numerical and experimental results. *Estuar. Coast Shelf Sci.* 53 (1), 25–38.
- Fairley, I., 2021. The potential and challenges of using drones to measure surface currents at tidal stream sites. In: *Supergen ORE Hub Annual Assembly*. Plymouth.
- Fairley, I., et al., 2013. Evaluation of tidal stream resource in a potential array area via direct measurements. *Renew. Energy* 57, 70–78.
- Fairley, I., et al., 2021. A preliminary assessment of the use of drones to quantify current velocities at tidal stream sites. In: *European Wave and Tidal Energy Conference 2021*. Plymouth.
- Fairley, I., et al., 2022. Drone-based large-scale particle image velocimetry applied to tidal stream energy resource assessment. *Renew. Energy* 196, 839–855.
- Farneback, G., 2003. *Two-Frame Motion Estimation Based on Polynomial Expansion*. Springer Berlin Heidelberg, Berlin, Heidelberg.
- Frost, C.H., et al., 2017. The impact of axial flow misalignment on a tidal turbine. *Renew. Energy* 113, 1333–1344.
- Fujita, I., Muste, M., Kruger, A., 1998. Large-scale particle image velocimetry for flow analysis in hydraulic engineering applications. *J. Hydraul. Res.* 36 (3), 397–414.
- Fujita, I., et al., 2019. Efficient and accurate estimation of water surface velocity in STIV. *Environ. Fluid Mech.* 19 (5), 1363–1378.
- Gacic, M., et al., 2009. Surface current patterns in front of the Venice Lagoon. *Estuar. Coast Shelf Sci.* 82 (3), 485–494.
- Geyer, N.L., et al., 2022. Drifter and dye tracks reveal dispersal processes that can affect phytoplankton distributions in shallow estuarine environments. *Estuar. Coast Shelf Sci.* 269.
- Goddijn-Murphy, L., Woolf, D.K., Easton, M.C., 2013. Current patterns in the inner Sound (Pentland Firth) from underway ADCP data. *J. Atmos. Ocean. Technol.* 30 (1), 96–111.
- González-Gorbeña, E., et al., 2018. Estimating the optimum size of a tidal array at a multi-inlet system considering environmental and performance constraints. *Appl. Energy* 232, 292–311.
- Heyman, J., 2019. TracTrac: a fast multi-object tracking algorithm for motion estimation. *Comput. Geosci.* 128, 11–18.
- Holman, R.A., Brodie, K.L., Spore, N.J., 2017. Surf zone characterization using a small quadcopter: technical issues and procedures. *IEEE Trans. Geosci. Rem. Sens.* 55 (4), 2017–2027.
- Kataoka, T., Hinata, H., Nihei, Y., 2013. Numerical estimation of inflow flux of floating natural macro-debris into Tokyo Bay. *Estuar. Coast Shelf Sci.* 134, 69–79.
- Keramea, P., et al., 2021. Oil spill modeling: a critical review on current trends, perspectives, and challenges. *J. Mar. Sci. Eng.* 9 (2).
- Khan, M.J., et al., 2009. Hydrokinetic energy conversion systems and assessment of horizontal and vertical axis turbines for river and tidal applications: a technology status review. *Appl. Energy* 86 (10), 1823–1835.
- Kim, D.J., Moon, W.M., Kim, Y.S., 2010. Application of TerraSAR-X data for emergent oil-spill monitoring. *IEEE Trans. Geosci. Rem. Sens.* 48 (2), 852–863.
- Klemas, V., 2012. Remote sensing of coastal and ocean currents: an overview. *J. Coast Res.* 28 (3), 576–586.
- Leitão, J.P., et al., 2018. Urban overland runoff velocity measurement with consumer-grade surveillance cameras and surface structure image velocimetry. *J. Hydrol.* 565, 791–804.
- Lewis, Q.W., Rhoads, B.L., 2015. Resolving two-dimensional flow structure in rivers using large-scale particle image velocimetry: an example from a stream confluence. *Water Resour. Res.* 51 (10), 7977–7994.
- Lewis, Q.W., Lindroth, E.M., Rhoads, B.L., 2018a. Integrating unmanned aerial systems and LSPIV for rapid, cost-effective stream gauging. *J. Hydrol.* 560, 230–246.
- Lewis, Q.W., Rhoads, B.L., 2018b. LSPIV measurements of two-dimensional flow structure in streams using small unmanned aerial systems: 1. Accuracy assessment based on comparison with stationary camera platforms and in-stream velocity measurements. *Water Resour. Res.* 54 (10), 8000–8018.
- Lieber, L., et al., 2019. Localised anthropogenic wake generates a predictable foraging hotspot for top predators. *Commun. Biol.* 2 (1), 123.
- Lieber, L., Langrock, R., Nimmo-Smith, W., 2021. A Bird's-Eye View on Turbulence: Seabird Foraging Associations with Evolving Surface Flow Features. *Proceedings of the Royal Society B: Biological Sciences*, p. 288.
- Lopez, G., et al., 2020. Surface Currents in the Alderney Race from High-Frequency Radar Measurements and Three-Dimensional Modelling. *Philosophical Transactions of the Royal Society a-Mathematical Physical and Engineering Sciences*, p. 378, 2178.
- McCann, D.L., Bell, P.S., 2014. Marine radar derived current vector mapping at a planned commercial tidal stream turbine array in the Pentland Firth, UK. In: *Oceans. IEEE, St Johns, Canada*.
- McIlvenny, J., et al., 2021. Combining acoustic tracking and hydrodynamic modelling to study migratory behaviour of Atlantic salmon (*Salmo salar*) smolts on entry into high-energy coastal waters. *ICES (Int. Coun. Explor. Sea) J. Mar. Sci.* 78 (7), 2409–2419.
- McIlvenny, J., et al., 2022. Comparison of dense optical flow and PIV techniques for mapping surface current flow in tidal stream energy sites. *Int. J. Energy Environ.* 14, 273–285.
- Mente, E., et al., 2006. Effect of feed and feeding in the culture of salmonids on the marine aquatic environment: a synthesis for European aquaculture. *Aquacult. Int.* 14 (5), 499–522.
- Murray, R.O., Gallego, A., 2017. A modelling study of the tidal stream resource of the Pentland Firth, Scotland. *Renew. Energy* 102, 326–340.
- OES-Environmental. Ramsey Sound, 2017 [cited 2021 29/11/2021]; Available from: <https://tethys.pnnl.gov/project-sites/ramsey-sound>.
- Omoniyi, G.E., et al., 2021. In-stream variability of litter breakdown and consequences on environmental monitoring. *Water (Switzerland)* 13 (16).
- Pearce, S., et al., 2020. An evaluation of image velocimetry techniques under low flow conditions and high seeding densities using unmanned aerial systems. *Rem. Sens.* 12 (2).
- Rusdiansyah, A., et al., 2018. The impacts of the large-scale hydraulic structures on tidal dynamics in open-type bay: numerical study in Jakarta Bay. *Ocean Dynam.* 68 (9), 1141–1154.
- Rüssmeier, N., Hahn, A., Zielinski, O., 2017. Ocean surface water currents by large-scale particle image velocimetry technique. In: *OCEANS 2017 - Aberdeen*.
- Schaefer, M., Woodyer, T., 2015. Assessing absolute and relative accuracy of recreation-grade and mobile phone GNSS devices: a method for informing device choice. *Area* 47 (2), 185–196.
- Schnauder, I., Anlanger, C., Koll, K., 2022. Wake flow patterns and turbulence around naturally deposited and installed trees in a gravel bed river. *Int. Rev. Hydrobiol.* 107 (1–2), 22–33.
- Sentchev, A., Forget, P., Barbin, Y., 2009. Residual and tidal circulation revealed by VHF radar surface current measurements in the southern Channel Isles region (English Channel). *Estuar. Coast Shelf Sci.* 82 (2), 180–192.
- Sentchev, A., et al., 2020. Underway Velocity Measurements in the Alderney Race: towards a Three-Dimensional Representation of Tidal Motions. *Philosophical Transactions of the Royal Society a-Mathematical Physical and Engineering Sciences*, p. 378, 2178.
- Sivas, D., Olcay, A.B., Ahn, H., 2015. Investigation of a corrugated channel flow with an open source PIV software. In: *10th Anniversary International Conference on Experimental Fluid Mechanics. CZECH REPUBLIC, Prague*.
- Slingsby, J., et al., 2021. Surface characterisation of kolk-boils within tidal stream environments using UAV imagery. *J. Mar. Sci. Eng.* 9 (5).
- Slingsby, J., et al., 2022. Using unmanned aerial vehicle (UAV) imagery to characterise pursuit-diving seabird association with tidal stream hydrodynamic habitat features. *Front. Mar. Sci.* 9.
- Sponaugle, S., et al., 2002. Predicting self-recruitment in marine populations: biophysical correlates and mechanisms. *Bull. Mar. Sci.* 70 (1), 341–375.
- Strelnikova, D., et al., 2020. Drone-based optical measurements of heterogeneous surface velocity fields around fish passages at hydropower dams. *Rem. Sens.* 12 (3).
- Streifer, M., Carrasco, R., Horstmann, J., 2017. Video-based estimation of surface currents using a low-cost quadcopter. *Geosci. Rem. Sens. Lett. IEEE* 14 (11), 2027–2031.
- Sutarto, T.E., 2015. Application of large scale particle image velocimetry (LSPIV) to identify flow pattern in a channel. *Procedia Eng.* 125, 213–219.
- Tauro, F., et al., 2015. Large-scale particle image velocimetry from an unmanned aerial vehicle. *IEEE ASME Trans. Mechatron.* 20 (6), 3269–3275.
- Tauro, F., Petroselli, A., Arcangeletti, E., 2016. Assessment of drone-based surface flow observations. *Hydrol. Process.* 30 (7), 1114–1130.
- Tauro, F., Piscopia, R., Grimaldi, S., 2019. PTV-Stream: a simplified particle tracking velocimetry framework for stream surface flow monitoring. *Catena* 172, 378–386.
- Thielicke, W., Stamhuis, E.J., 2014. PIVlab – towards user-friendly, affordable and accurate digital particle image velocimetry in MATLAB. *J. Open Res. Software* 2 (1), 30.
- Thielicke, W., Sonntag, R., 2021. Particle image velocimetry for MATLAB: accuracy and enhanced algorithms in PIVlab. *J. Open Res. Software* 9 (1), 12.
- Togneri, M., Masters, I., 2016. Micrositing variability and mean flow scaling for marine turbulence in Ramsey Sound. *Journal of Ocean Engineering and Marine Energy* 2 (1), 35–46.
- Townshend, A.D., Worringham, C.J., Stewart, I.B., 2008. Assessment of speed and position during human locomotion using nondifferential GPS. *Med. Sci. Sports Exerc.* 40 (1), 124–132.
- Tsubaki, R., Fujita, I., Tsutsumi, S., 2011. Measurement of the flood discharge of a small-sized river using an existing digital video recording system. *Journal of Hydro-Environment Research* 5 (4), 313–321.
- Ubelmann, C., et al., 2021. Reconstructing Ocean surface current combining altimetry and future spaceborne Doppler data. *J. Geophys. Res.: Oceans* 126 (3), e2020JC016560.
- Uncles, R.J., 2010. Physical properties and processes in the Bristol Channel and severn estuary. *Mar. Pollut. Bull.* 61 (1), 5–20.

- Waggitt, J.J., et al., 2016. Quantifying pursuit-diving seabirds' associations with fine-scale physical features in tidal stream environments. *J. Appl. Ecol.* 53 (6), 1653–1666.
- Ward, S., 2018. Tidal energy assessment of Strumble Head, with a novel focus on floating tidal stream energy converters. In: SEACAMS2 R&D Report. Bangor University.
- Willis, M., et al., 2010. Tidal turbine deployment in the Bristol Channel: a case study. *Proceedings of the Institution of Civil Engineers - Energy* 163 (3), 93–105.
- Wilson, G., Berezchnoy, S., 2018. Surfzone state estimation, with applications to quadcopter-based remote sensing data. *J. Atmos. Ocean. Technol.* 35 (10), 1881–1896.
- Witte, T.H., Wilson, A.M., 2004. Accuracy of non-differential GPS for the determination of speed over ground. *J. Biomech.* 37 (12), 1891–1898.
- Witte, T.H., Wilson, A.M., 2005. Accuracy of WAAS-enabled GPS for the determination of position and speed over ground. *J. Biomech.* 38 (8), 1717–1722.
- Wyatt, L., 2018. Wave and tidal power measurement using HF radar. *International Marine Energy Journal* 1.
- Zhu, X., Lipeme Kouyi, G., 2019. An analysis of LSPIV-based surface velocity measurement techniques for stormwater detention basin management. *Water Resour. Res.* 55 (2), 888–903.
- Zuiderverld, K., 1994. In: Heckbert, P. (Ed.), *Contrast Limited Adaptive Histogram Equalisation*. Graphic Gems IV. Academic Press Professional, San Diego.